Involvement of the Toll-like receptor 4 pathway and use of TNF-α antagonists for treatment of the mucopolysaccharidoses

Calogera M. Simonaro[a,1], Yi Ge[a], Efrat Eliyahu[a], Xingxuan He[a], Karl J. Jepsen[b], and Edward H. Schuchman[a]

Departments of [a]Genetics and Genomic Sciences and [b]Orthopaedics, Mount Sinai School of Medicine, New York, NY 10029

Communicated by William S. Sly, Saint Louis University School of Medicine, St. Louis, MO, November 10, 2009 (received for review August 20, 2009)

Enzyme replacement therapy is currently available for three of the mucopolysaccharidoses (MPSs) but has limited effects on the skeletal lesions. We investigated the involvement of the Toll-like receptor 4 (TLR4) signaling pathway in the pathogenesis of MPS bone and joint disease, and the use of the anti-TNF-α drug, Remicade (Centocor, Inc.), for treatment. TLR4 KO (TLR4$^{(lps-/-)}$) mice were interbred with MPS VII mice to produce double-KO (DKO) animals. The DKO mice had longer and thinner faces and longer femora as revealed by micro-computed tomography analysis compared with MPS VII mice. Histological analyses also revealed more organized and thinner growth plates. The serum levels of TNF-α were normalized in the DKO animals, and the levels of phosphorylated STAT1 and STAT3 in articular chondrocytes were corrected. These findings led us to evaluate the effects of Remicade in MPS VI rats. When initiated at 1 month of age, i.v. treatment prevented the elevation of TNF-α, receptor activator of NF-κB, and other inflammatory molecules not only in the blood but in articular chondrocytes and fibroblast-like synoviocytes (FLSs). Treatment of 6-month-old animals also reduced the levels of these molecules to normal. The number of apoptotic articular chondrocytes in MPS VI rats was similarly reduced, with less infiltration of synovial tissue into the underlying bone. These studies revealed the important role of TLR4 signaling in MPS bone and joint disease and suggest that targeting TNF-α may have positive therapeutic effects.

bone and joint disease | inflammation | glycosaminoglycans | growth plate

The mucopolysaccharidoses (MPSs) comprise a family of 11 enzyme deficiencies that result in defective catabolism of glycosaminoglycans (GAGs) (1, 2). Because GAG metabolism is important for connective tissue function, the MPS disorders manifest with severe connective tissue disease. However, despite the fact that skeletal abnormalities are the most debilitating feature of these disorders, there have been few investigations into the underlying mechanisms leading to MPS bone and joint disease. Our laboratory has used MPS animal models to document the molecular, biochemical, and cellular changes occurring in these tissues. We reported that GAG storage in MPS induces a complex sequence of molecular abnormalities, leading to inflammation, apoptosis (cartilage), and hyperplasia (synovial membranes), which result in poorly organized and metabolically abnormal connective tissue matrices (3–5).

We also hypothesized that lysosomal and/or extracellular GAG storage in the MPS disorders induces inflammation and altered growth of connective tissue and other cells through activation of the Toll-like receptor 4 (TLR4) signaling pathway (5). This concept was recently supported by the findings of Ausseil et al. (6), who demonstrated priming of microglia via the TLR4 pathway in the brains of MPS IIIB mice. In addition to heparan sulfate fragments, gangliosides accumulate in the brains of MPS IIIB mice, and it is possible that gangliosides and/or other storage products in connective tissue cells may also contribute to TLR4 activation.

Metcalf et al. (7) recently showed that mRNAs encoding several STAT transcription factors known to be selectively altered by inflammation were abnormally expressed in the growth plates of MPS VII mice. In particular, p-STAT3-Tyr705, a proproliferative factor, was decreased in MPS VII mice and p-STAT1-Ser727, an antiproliferative factor, was elevated. Tessitore et al. (8) also reported elevated inflammation and apoptosis in MPS VI human fibroblasts as well as impaired autophagy.

TLR4 stimulates a complex array of downstream events that lead to cell death in some circumstances and cell proliferation in others (9). TLR4 signaling may be induced by two pathways (10, 11). LPS represents the "classic" pathway, activating TLR4 signaling through interactions with the adapter protein, myeloid differentiation factor-88 (MyD88), LPS binding protein (LBP), CD14, and CXCR4 (12). Hyaluronan fragments and oligosaccharides released from the breakdown of the extracellular matrices also have been shown to signal through TLR4 via MyD88 and CD44 (11), providing further support for the concept that GAG storage in the MPS disorders activates this pathway.

Enzyme replacement therapy (ERT) is currently available for three MPS disorders (MPS I, II, and VI). However, despite the fact that animal models have shown improvements in bone and/or joint disease if ERT was initiated early, few clinical improvements in bone disease have been observed in patients (13–15). Thus, unique treatment strategies are necessary for patients with MPS, particularly for the bones and joints. We have shown that TLR4 activation in MPS animals resulted in the production of the proapoptotic lipid, ceramide, and the release of numerous inflammatory cytokines and proteases (5). Among the cytokines, TNF-α was markedly elevated both in the circulation and within the joint tissue of MPS animals (5).

The current study had two goals. First, we sought to document the physiological importance of TLR4 signaling in MPS bone and joint disease using a genetic approach by breeding TLR4 KO mice to MPS VII mice, and, second, we evaluated the effects of treating TNF-α release using the US Food and Drug Administration (FDA)-approved drug, Remicade (Centocor, Inc.). The results of these studies are described herein.

Results and Discussion

TLR4 signaling may be induced either by LPS or by endogenous GAG fragments derived from the breakdown of extracellular matrix components (10, 11) (Fig. 1*A*). We previously showed that the expression of MyD88, LBP, and CD14 was up-regulated in MPS connective tissue cells, leading to activation of the "LPS-specific" TLR4 pathway (5). This activation resulted in the release

Author contributions: C.M.S. and E.H.S. designed research; C.M.S., Y.G., E.E., X.H., and K.J.J. performed research; C.M.S. and E.H.S. analyzed data; and C.M.S. wrote the paper.

The authors declare no conflict of interest.

Freely available online through the PNAS open access option.

[1]To whom correspondence should be addressed at: Department of Genetics and Genomic Sciences, Mount Sinai School of Medicine, 1425 Madison Avenue, Room 14-20C, New York, NY 10029. E-mail: calogera.simonaro@mssm.edu.

This article contains supporting information online at www.pnas.org/cgi/content/full/0912937107/DCSupplemental.

of inflammatory cytokines, proteases, and growth factors at the sites of pathology (e.g., bone and cartilage) and into the circulation. To investigate activation of the "GAG-specific" pathway, we determined the levels of CD44 in MPS VI rat fibroblast-like synoviocytes (FLSs) and articular chondrocytes and found that the expression of CD44 also was substantially elevated in MPS cells (Fig. 1*B*). Thus, in MPS connective tissue, TLR4 activation occurs via both the LPS- and GAG-specific pathways.

To examine TLR4 expression in MPS connective tissue cells further, immunolocalization studies were carried out using MPS VI rat FLSs (Fig. 2*A*). Consistent with our prior data (5), these results revealed a high level of TLR4 colocalization in MPS lysosomes, likely attributable to accumulation within these dysfunctional organelles.

Abnormal lysosomal and/or endosomal trafficking occurs in many lysosomal storage disorders, leading to enhanced apoptosis and/or altered autophagy (16, 17). Autophagy is an important normal function of the lysosomal/endosomal system and has been shown to protect cells from inflammation caused by oxidative stress (18). Because growth plate and articular chondrocytes are embedded in an avascular environment with a limited oxygen supply, they particularly rely on autophagy to sustain cell survival (19).

To examine autophagy in MPS, the levels of microtubule-associated protein 1 light chain 3 (LC3-I) and its phosphatidylethanolamine-conjugated form (LC3-II) were determined. Conversion of LC3-I to LC3-II is a marker of autophagosome formation (20). As shown in Fig. 2*B*, MPS VI rat FLSs accumulate LC3-I predominantly, indicating little autophagosome formation. In contrast, in MPS VI articular chondrocytes, LC3-I was completely converted to LC3-II, suggesting an increased number of autophagosomes. These data are consistent with previous findings indicating that these two different MPS connective tissue cell types have distinct pathological changes. Tessitore et al. (8) also have shown that human MPS VI skin fibroblasts accumulate LC3-II.

To examine the physiological significance of TLR4 activation in the MPS disorders genetically, TLR4$^{(lps-/-)}$ mice were bred to MPS VII mice to generative double-KO (DKO) mice. As shown in Fig. 3*A* and Fig. S1*A*, inactivation of TLR4 in MPS VII mice had a significant positive effect on their growth. Quantitative analysis similarly revealed longer and thinner faces in the DKO mice when compared with MPS VII mice (Fig. 3*B*).

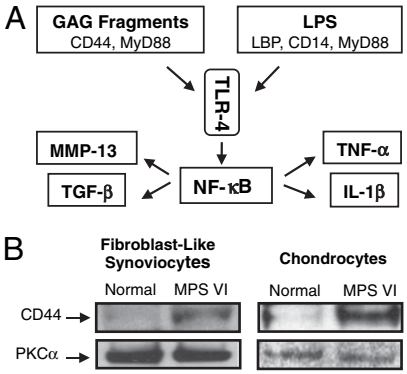

Fig. 1. (*A*) TLR4 signaling pathway can be activated via GAG fragments requiring CD44 and MyD88 or through LPS, which requires MyD88, LBP, and CD14. (*B*) CD44 adhesion receptor (55 kDa) is a hyaluronan-binding cell surface glycoprotein involved in the initiation of GAG-induced inflammation via TLR4. Elevated CD44 expression was detected in 6-month-old MPS VI rat FLSs and articular chondrocytes, confirming the activation of TLR4 via the GAG pathway in MPS. Protein kinase C-α (PKC-α; 82 kDa) was used as a loading control.

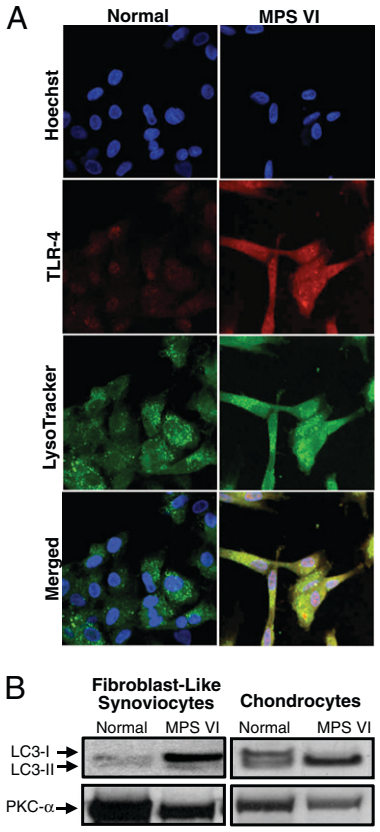

Fig. 2. Localization of TLR4 in MPS VI lysosomes. (*A*) Rat FLSs were incubated with TLR4 primary polyclonal anti-rat antibody and LysoTracker Green to visualize lysosomes. Visualization of TLR4 was accomplished using a fluorescent secondary antibody, Cy-3, and nuclei were stained with a bisbenzamide Hoechst dye. Note the elevated levels of TLR4 in MPS VI cells and colocalization with the LysoTracker Green dye. (*B*) Anti-LC3-I (14 kDa) and LC3-II (16 kDa) Western blots of FLSs and articular chondrocytes from 6-month-old normal and MPS VI rats showing the lack of conversion of the LC3-I isoform to LC3-II in the FLSs. In contrast, in MPS VI articular chondrocytes, LC3-I was completely converted to LC3-II. Protein kinase C-α (Pkc-α) was used as a loading control.

We also assessed the effects of TLR4 KO on the bones of MPS VII mice by micro-computed tomography (CT) imaging and histological analysis of their growth plates. Micro-CT revealed longer femora in the DKO mice compared with age- and gender-matched MPS VII mice (Fig. 3*C*), despite the fact that an osteopetrotic phenotype was still observed and bone density was unchanged in the DKO mice. Fig. S1*A* graphically depicts the femur and tibia lengths for all the MPS VII and DKO mice analyzed. Both the femora and tibias of TLR4$^{(lps-/-)}$ control mice were equivalent to those of age- and gender-matched WT mice.

We also found that the growth plates of MPS VII mice were thicker and more disorganized when compared with those of TLR4$^{(lps-/-)}$ mice and were improved in the DKO mice (Fig. 3*D* and Fig. S1*B*). However, despite these improvements, the enlarged cells in the MPS VII growth plates remained in the DKO mice. This may be expected, because the increased cell size in MPS is likely attributable to GAG storage, which would not be affected by TLR4 KO.

We also observed no differences in total cell numbers in the MPS VII vs. control growth plates (Fig. S1*C*). This contrasts with recent findings by Metcalf et al. (7), who showed reduced cell numbers in the proliferative zone of MPS VII mice. This difference may be attributable to the fact that the mice in that study

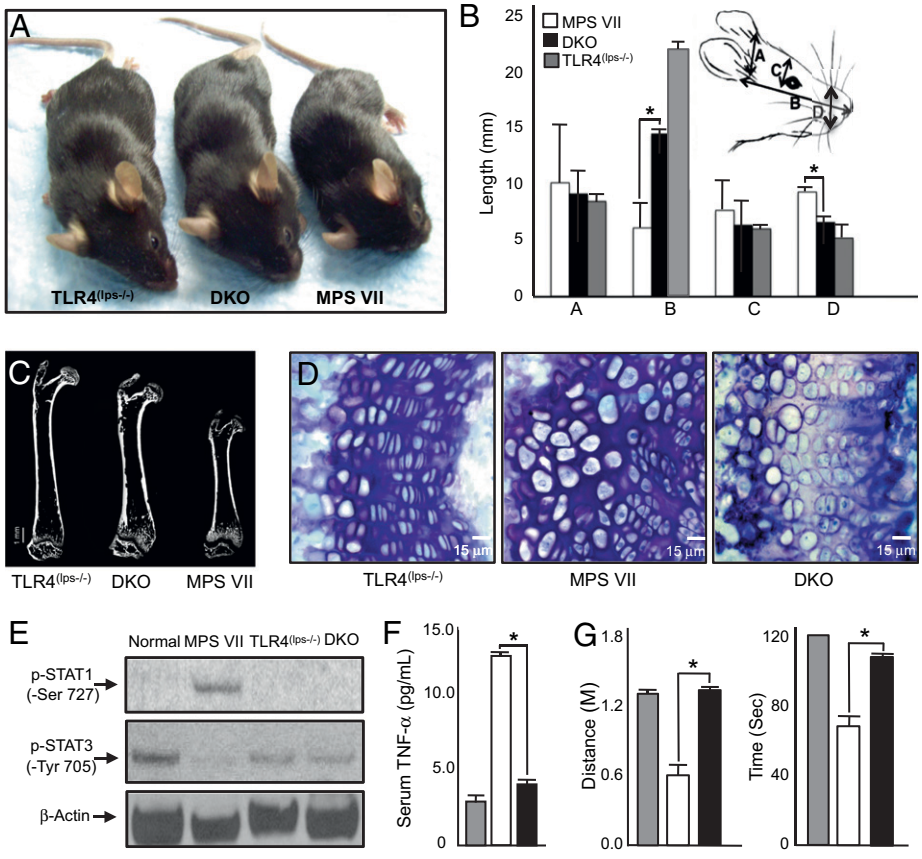

Fig. 3. (*A*) MPS VII and TLR4$^{(lps-/-)}$ mice were crossed to produce a double-mutant (DKO) strain (MPS VII/TLR4$^{(lps-/-)}$). Note the dramatic size difference between MPS VII and DKO mice. Shown are representative 5-month-old TLR4$^{(lps-/-)}$, DKO, and MPS VII male mice. (*B*) Skull measurements, including width (A), length (B), inner canthal distance (C), and nose widths (D), were taken of age- and gender-matched TLR4$^{(lps-/-)}$, DKO, and MPS VII male mice ($n = 6$). TLR4$^{(lps-/-)}$ mice had skull measurements that were equivalent to normal. A significant increase in skull length and reduction in width were observed in the DKO mice compared with the MPS VII mice. *$P < 0.001$. (*C*) Micro-CT analysis was performed on femora from TLR4$^{(lps-/-)}$, DKO, and MPS VII male mice ($n = 6$). A representative image is shown, revealing that the bones were significantly longer in DKO vs. MPS VII mice. (*D*) Representative images of the growth plates from TLR4$^{(lps-/-)}$, MPS VII, and DKO mice. Note that the growth plates were thinner in DKO vs. MPS VII mice and that the columns were more organized. (Scale bar: 15 μm.) (*E*) Levels of p-STAT1-Ser727 (90 kDa) and p-STAT3-Tyr705 (90 kDa) were analyzed by Western blotting in normal, MPS VII, TLR4$^{(lps-/-)}$, and DKO mice. β-Actin was used as a loading control (46 kDa). MPS VII mice had elevated p-STAT1-Ser727 and reduced p-STAT3-Tyr705; these were corrected in the DKO mice. (*F*) TNF-α serum levels were analyzed by ELISA in 5-month-old TLR4$^{(lps-/-)}$ (gray bar), MPS VII (white bar), and DKO (black bar) mice ($n = 6$). Significantly elevated TNF-α levels were evident in the MPS VII mice, which were normalized in the DKO mice. (*G*) Male 5-month-old TLR4$^{(lps-/-)}$ (gray bar), MPS VII (white bar), and DKO (black bar) mice were placed on an accelerating rotarod to assess coordination and mobility ($n = 6$). The MPS VII mice could not complete the task and fell off between 54 (0.38 m) and 75 (0.70 m) sec after initiating the run. In contrast, the DKO mice completed the 120-sec (1.4 m) task, equivalent to the control TLR4$^{(lps-/-)}$ mice. *$P < 0.001$.

were 3 weeks of age, whereas they were 6 weeks of age in this study. This difference in age can have a major impact on growth plate development. For example, Ahmed et al. (21) have shown that a secondary proliferative cluster of cells appears at 4 weeks in the growth plates of "Tich" mice, leading to increased thickness. In this model, as in MPS, these cells are dysfunctional and do not result in calcification or bone growth. Given that cell size and number were unchanged in the DKO animals, we hypothesize that the improved bone length and size of the DKO vs. MPS VII mice may be the result of increased endochondral ossification attributable to improved chondrocyte alignment within the growth plate columns, contributing to a reduction in growth plate width.

We next assessed the levels of phosphorylated STAT1 and STAT3 in normal, TLR4$^{(lps-/-)}$, MPS VII, and DKO articular chondrocytes by Western blot analysis (Fig. 3*E*). As reported by others (7), MPS VII mice had elevated levels of p-STAT1-Ser727 and repressed levels of p-STAT3-Tyr705, consistent with activation of TLR4. The levels of p-STAT1-Ser727 and 3-Tyr705 in the DKO mice were normal, indicating that inactivation of the TLR4 pathway in MPS VII mice corrected the abnormal pSTAT1 and pSTAT3 expression.

Similar alterations in STAT1 and STAT3 have been observed in rheumatoid arthritis (RA) and have been attributed to activation of TNF-α (22–24). We therefore assessed the serum levels of TNF-α. The elevated levels seen in MPS VII mice were normalized in DKO mice (Fig. 3*F*). TNF-α is an important downstream mediator of TLR4, and several investigators have recently shown that TLR4 activation and/or TNF-α has important pathogenic effects in the brains of MPS mouse models (6, 25). We therefore examined the locomotor behavior of the DKO mice using an accelerating rotarod (Fig. 3*G*). At 5 months of age, the performance of the DKO mice on the rotarod was equivalent to that of control TLR4$^{(lps-/-)}$ mice, in contrast to MPS VII mice, which were markedly defective. Although these results are consistent with improved cerebellar function in the DKO mice, rotarod locomotion is a complex task and the results could also relate partially or wholly to improvements in the bones and joints.

The data presented above demonstrate the important role of TLR4 in the pathogenesis of MPS VII bone and joint disease and show that inhibition of this pathway has a significant positive effect. Currently there are no FDA-approved drugs that directly target TLR4, although Remicade, which targets TNF-α, has been approved for use in RA and other inflammatory diseases (26–29). Remicade is a chimeric monoclonal antibody against human TNF-α that has been shown to cross-react in rats and other species (30, 31). In RA, it reduces the levels of circulating TNF-α, leading to improvement in joint lesions (32, 33). Because TNF-α is a major cytokine released in MPS animals (3, 4), we evaluated the effectiveness of this drug in alleviating inflammation and its downstream effects. Two groups of MPS VI rats were treated with Remicade. Group 1 animals were 6 months of age, had significantly elevated TNF-α, and had established bone and joint disease. Group 2 animals were 1 month of age, had normal levels of TNF-α, and were presymptomatic.

As shown in Fig. 4*A*, Remicade treatment of group 1 rats for 8 weeks reduced their serum TNF-α levels to normal. Treatment of group 2 rats for 24 weeks maintained their serum TNF-α at normal. Previously, we found that MPS VI rats also had elevated serum levels of receptor activator of NF-κB (RANKL) (4). This inflammatory molecule has many potential pathological effects, including a potent effect on osteoclastogenesis (34). As shown in Fig. 4*B*, treatment of MPS VI rats with Remicade also substantially reduced the levels of serum RANKL in group 1 and maintained normal levels in group 2. The reduction of TNF-α and RANKL in group 1 represents a true reversal of inflammation, whereas group 2 showed prevention. We also determined the plasma levels of two signaling lipids, ceramide and sphingosine-1-phosphate (S1P), in treated MPS VI rats. Ceramide is a proapoptotic lipid that contributes to the cell death observed in MPS articular chondrocytes. S1P is a "proliferative" lipid that contributes to the hyperplasia seen in MPS synovial tissue (5). As we have described, both lipids are elevated in MPS VI rats and both were normalized in the treated group 1 animals (6 months old) (Fig. 4*C*).

To examine the effects of Remicade in the joints of MPS VI animals, we obtained FLSs pre- and posttreatment and studied the expression of COX-2, p38, TGF-β, and sphingosine-1-kinase (Sphk1). We have previously shown elevated levels of COX-2, p38, and TGF-β in MPS FLSs, each of which is a downstream mediator of TNF-α. Sphk1 is an enzyme responsible for the production of S1P. As shown in Fig. 4*D*, following 8 weeks of Remicade treatment of 6-month-old MPS VI rats, the levels of these four molecules were reduced to normal in the FLSs.

Clinically, the appearance, weight, and length of the treated MPS VI rats were not significantly different from those of untreated animals. This is consistent with the fact that the stored GAGs and GAG fragments in the growth plate cells were not being reduced and/or the growth plate changes may already be irreversible after 1 month of age. Further, Remicade inhibits TNF-α in the serum, and the growth plate is an extremely avascular tissue. Nonetheless, TUNEL staining of the articular cartilage in the treated rats showed an ~50% reduction in the apoptotic index compared with untreated MPS VI rats (Fig. 4*E*), resulting in levels that were close to normal. There was also less invasion of the synovial tissue into the underlying bone.

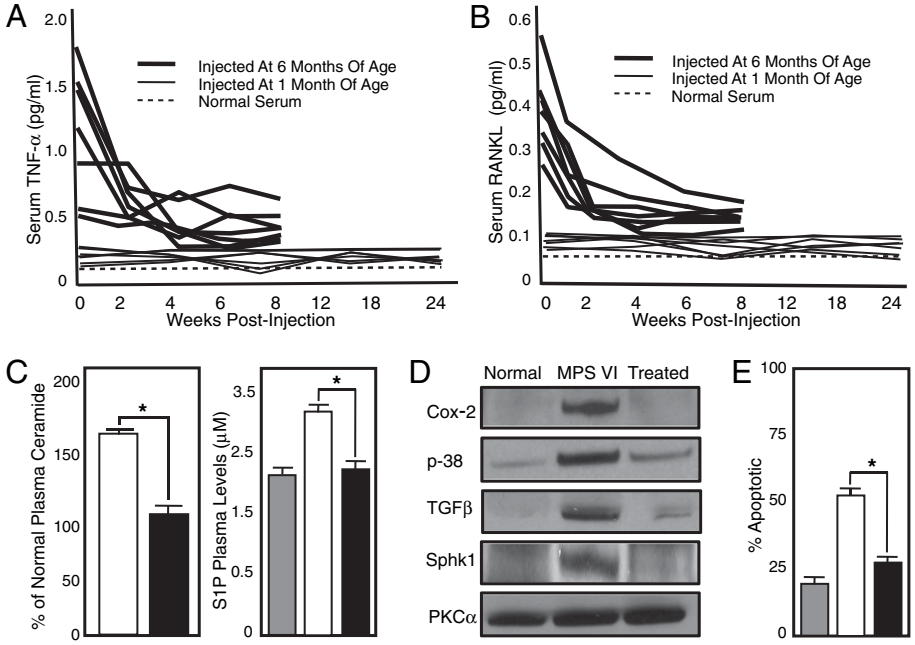

Fig. 4. Six-month-old MPS VI rats ($n = 7$) with advanced bone disease and 1-month-old presymptomatic MPS VI rats ($n = 7$) were injected i.v. with 3 mg/kg of Remicade every third day for 8 weeks in the older animals and 24 weeks in the younger group. Serum was collected every 2 weeks in the treated animals. (*A*) Remicade treatment prevented the elevation of circulating TNF-α in the presymptomatic group, although the levels were normalized in the animals with advanced disease. (*B*) Similar response was seen in serum RANKL levels, indicating that inhibition of TNF-α was having downstream effects. (*C*) Ceramide and S1P plasma levels were measured in normal (gray bar), untreated 8-month-old MPS VI (white bar), and MPS VI rats that were treated for 8 weeks beginning at 6 months of age (black bar). Note the reduced levels of both bioactive lipids in the MPS VI-treated animals. (*D*) Posttreatment, FLSs were isolated from the MPS VI rats as well as age-matched normal and untreated MPS VI animals. The expression of two molecules that are activated by TNF-α, cyclooxygenase-2 (COX-2; 73 kDa) and p38 (38-kDa), were examined by Western blot analysis. Note that the levels of both proteins were normalized in the treated MPS VI cells. In addition, the expression of TGF-β (30 kDa) and Sphk1 (54 kDa) were normalized in the treated animals. Protein kinase C-α (82 kDa) was used as a loading control. (*E*) Apoptotic (TUNEL) staining of articular cartilage was performed after 24-week treatment in MPS VI animals. Two hundred cells were counted per animal. Fifty-five percent TUNEL-positive cells were found in the untreated animals (white bar) vs. 29% in the treated animals (black bar). $*P < 0.01$. The differences between normal (gray bar) and treated MPS VI rats were not statistically significant.

From these studies, we conclude that activation of the TLR4 pathway in the MPS disorders, likely a direct consequence of GAG storage, has major pathological effects on the joints and bones. Inactivation of this pathway in MPS VII/TLR4$^{(lps-/-)}$ DKO mice corrects many biochemical and clinical features of the disease, suggesting that drugs targeting this pathway could be effective in the treatment of these disorders. TLR4 activation leads to the elevation of TNF-α, and Remicade, an FDA-approved anti-TNF-α drug, can attenuate the inflammatory response in MPS VI animals, leading to improved joint pathology. We propose that this and related antiinflammatory treatments should be evaluated in MPS patients, alone or in conjunction with ERT. In addition to their direct effects on MPS pathology, such drugs may, by reducing inflammation, increase the accessibility of synovial tissues to recombinant proteins and improve the efficacy of ERT.

Materials and Methods

Additional information is provided in *SI Materials and Methods*.

Animals. ***Mice.*** MPS VII, B6, and TLR4$^{(lps-/-)}$ (Jackson Laboratory) mice have been previously described (35–37). MPS VII and TLR4$^{(lps-/-)}$ mice were interbred to obtain DKO animals. The growth, size, and lifespan of TLR4$^{(lps-/-)}$ mice were the same as for WT B6 mice, and the TLR4$^{(lps-/-)}$ mice were therefore used as normal controls in most instances (for details, see *SI Materials and Methods*).
Rats. The MPS VI rats have been previously described (38, 39).

Bone Measurements. Skull and limb measurements were taken of 5-month-old DKO, WT, MPS VII, and TLR4$^{(lps-/-)}$ mice (for details, see *SI Materials and Methods*).

Growth Plate Histology. Femora from 6-week-old DKO, WT, MPS VII, and TLR4$^{(lps-/-)}$ mice were fixed, embedded, sectioned, and stained with toluidine blue (for details, see *SI Materials and Methods*).

Micro-CT Analysis. 3D images of 6-week-old femora from MPS VII, TLR4$^{(lps-/-)}$, and DKO mice were obtained using an eXplore Locus SP PreClinical Specimen micro-CT system (GE Healthcare) (for details, see *SI Materials and Methods*).

Rotarod Analysis. Five-month-old male TLR4$^{(lps-/-)}$, MPS VII, and DKO mice were placed on an accelerating Rotarod series 8 (IITC Life Science) (for details, see *SI Materials and Methods*).

Immunblot Analysis of STAT Proteins. For analysis of p-STAT1 and p-STAT3 in articular chondrocytes from normal, MPS VII, TLR4$^{(lps-/-)}$, and DKO mice, cell extracts were prepared for immunoblot analysis as previously described with appropriate primary and secondary antibodies (5) (for details, see *SI Materials and Methods*).

TLR4 Immunolocalization Studies. Normal and MPS VI rat FLSs were cultured on coverslips, fixed with 4% (v/v) paraformaldehyde/PBS, incubated overnight with primary TLR4 antibody (Santa Cruz Biotechnology), and then incubated with the appropriate secondary antibody (4, 5). LysoTracker Green (Invitrogen) was used to visualize lysosomes and bis-benzamide Hoechst dye (Sigma–Aldrich) was used to visualize nuclei (for details, see *SI Materials and Methods*).

Autophagy Analyses. Expression of the autophagy markers LC3-I and LC3-II was assessed in normal and MPS VI FLSs obtained from 6-month-old rats using anti-rabbit LC3A/B antibodies (Abcam, Inc.). Cell extracts and blots were prepared as described above for analysis of the STAT proteins (for details, see *SI Materials and Methods*).

Remicade Treatment of MPS VI Rats. Six-month-old MPS VI rats (group 1) with advanced bone disease and 1-month-old presymptomatic MPS VI rats (group 2) were injected i.v. with 3 mg/kg of Remicade every third day for 8 and 24 weeks, respectively. Serum was collected every 2 weeks for TNF-α and RANKL analysis (see below). For each group ($n = 7$), the treated animals were killed 2 weeks after the last drug injection.

Humeri, femora, and tibias were collected from age-matched normal, untreated MPS VI, and treated MPS VI rats and placed in PBS for the isolation of FLSs and articular chondrocyte or fixed in neutral buffered 10% (v/v) formalin (Sigma Chemical) for immunohistochemistry (see below). The fixed bones were decalcified in 8% (v/v) formic acid (Sigma Chemical) for 5 days, paraffin-embedded, sectioned (5 μm), and stained with H&E or TUNEL. Primary FLS and articular chondrocyte cultures were established as previously described (4, 5), and expression of molecules involved in TLR4 signaling and autophagy was assessed (see above).

Analysis of the TLR4 Pathway in Remicade-Treated MPS VI Rats. The TLR4 pathway was assessed in FLSs and articular chondrocytes from 8-month-old normal, MPS VI, and treated MPS VI rats. Cell extracts and blots were prepared as previously described (4, 5). The membranes were incubated with anti-CD44, anti-COX-2, anti-p38, anti-Sphk1, and anti-protein kinase C-α (Santa Cruz Biotechnology) as a loading control. The bound antibodies were recognized by secondary antibodies conjugated to HRP (GE Healthcare). Detection of the antibody complexes was accomplished using an enhanced chemiluminescence detection reagent (Amersham Biosciences) (for details, see *SI Materials and Methods*).

TUNEL Staining in Remicade-Treated Rats. Apoptosis in tissue sections from control and treated MPS VI rats was assessed using the DNA terminal transferase nick-end translation method (TUNEL assay) as described (3). Apoptotic nuclei were visualized using a Nikon Eclipse E800 microscope (Nikon). To determine the percentage of apoptotic cells in the tissue sections from each group, at least 200 cells per animal were counted and the percentage of TUNEL-positive cells was scored.

Serum Immunoassays. TNF-α and RANKL activities were quantified in normal, MPS VI, and Remicade-treated MPS VI rat serum by immunoassays using rat ultrasensitive Biosource Elisa kits (Invitrogen and ALPCO Diagnostics) according to the manufacturers' protocols. TNF-α was quantified in serum from 5-month-old normal, TLR4$^{(lps-/-)}$, MPS VII, and DKO mice using a mouse Elisa kit (Invitrogen) according to the manufacturer's protocols. All assays were performed in triplicate.

Ceramide and SIP Quantification. Plasma from normal, MPS VI, and Remicade-treated MPS VI rats was collected at the end of the 8- and 24-week treatment periods, respectively. Plasma ceramide was quantified using the diacylglycerol kinase method (40). S1P was quantified using HPLC methods after napthalene-2,3-dicarboxaldehyde derivatization (41).

Data Presentation and Statistical Analyses. All experiments were independently replicated at least three times. The data between two groups were subjected to Student's t test analysis, and the results were considered significant at $P < 0.001$–0.002. Statistics were performed using Sigma Stat 3.1 (Systat Software). Graphs represent the mean ± SEM of combined data from the triplicate experiments.

ACKNOWLEDGMENTS. We thank Dr. Mark Haskins (University of Pennsylvania) for his careful review and comments on this manuscript. We also acknowledge Joseph Fusco and Valerie Williams for assistance with the growth plate and micro-CT analyses. This work was supported by grants from the National Institutes of Health (5R01DK25759, 1R01DK087185, and RR02512), the National Mucopolysaccharidoses Society, and the Isaac Foundation.

1. Neufeld EF, Meunzer J (2001) The mucopolysaccharidoses. *Metabolic and Molecular Basis of Inherited Disease*, eds Scriver CR, Beaudet Al, Sly WS, Valle D (McGraw–Hill, New York), pp 3421–3452.
2. Clarke LA (2008) The mucopolysaccharidoses: A success of molecular medicine. *Expert Rev Mol Med* 10:e1.
3. Simonaro CM, Haskins ME, Schuchman EH (2001) Articular chondrocytes from animals with a dermatan sulfate storage disease undergo a high rate of apoptosis and release nitric oxide and inflammatory cytokines: A possible mechanism underlying degenerative joint disease in the mucopolysaccharidoses. *Lab Invest* 81:1319–1328.
4. Simonaro CM, D'Angelo M, Haskins ME, Schuchman EH (2005) Joint and bone disease in mucopolysaccharidoses VI and VII: Identification of new therapeutic targets and biomarkers using animal models. *Pediatr Res* 57:701–707.
5. Simonaro CM, et al. (2008) Mechanism of glycosaminoglycan-mediated bone and joint disease: Implications for the mucopolysaccharidoses and other connective tissue diseases. *Am J Pathol* 172:112–122.
6. Ausseil J, et al. (2008) Early neurodegeneration progresses independently of microglial activation by heparan sulfate in the brain of mucopolysaccharidosis IIIB mice. *PLoS One* 3:e2296.

7. Metcalf JA, Zhang Y, Hilton MJ, Long F, Ponder KP (2009) Mechanism of shortened bones in mucopolysaccharidosis VII. *Mol Genet Metab* 97:202–211.
8. Tessitore A, Pirozzi M, Auricchio A (2009) Abnormal autophagy, ubiquitination, inflammation and apoptosis are dependent upon lysosomal storage and are useful biomarkers of mucopolysaccharidosis VI. *PathoGenetics* 2:4.
9. Triantafilou M, Triantafilou K (2002) Lipopolysaccharide recognition: CD14, TLRs and the LPS-activation cluster. *Trends Immunol* 23:301–304.
10. Hoshino K, et al. (1999) Cutting edge: Toll-like receptor 4 (TLR4)-deficient mice are hyporesponsive to lipopolysaccharide: Evidence for TLR4 as the Lps gene product. *J Immunol* 162:3749–3752.
11. Taylor KR, et al. (2007) Recognition of hyaluronan released in sterile injury involves a unique receptor complex dependent on Toll-like receptor 4, CD44, and MD-2. *J Biol Chem* 282:18265–18275.
12. Xia Y, Yamagata K, Krukoff TL (2006) Differential expression of the CD14/TLR4 complex and inflammatory signaling molecules following i.c.v. administration of LPS. *Brain Res* 1095:85–95.
13. Vogler C, et al. (1999) Enzyme replacement in murine mucopolysaccharidosis type VII: Neuronal and glial response to β-glucuronidase requires early initiation of enzyme replacement therapy. *Pediatr Res* 45:838–844.
14. Sly WS (2004) Enzyme replacement therapy for lysosomal storage disorders: Successful transition from concept to clinical practice. *Mo Med* 101:100–104.
15. Rohrbach M, Clarke JT (2007) Treatment of lysosomal storage disorders: Progress with enzyme replacement therapy. *Drugs* 67:2697–2716.
16. Settembre C, Fraldi A, Rubinsztein DC, Ballabio A (2008) Lysosomal storage diseases as disorders of autophagy. *Autophagy* 4:113–114.
17. Raben N, Shea L, Hill V, Plotz P (2009) Monitoring autophagy in lysosomal storage disorders. *Methods Enzymol* 453:417–449.
18. Scherz-Shouval R, et al. (2007) Reactive oxygen species are essential for autophagy and specifically regulate the activity of Atg4. *EMBO J* 26:1749–1760.
19. Srinivas V, Bohensky J, Zahm AM, Shapiro IM (2009) Autophagy in mineralizing tissues: Microenvironmental perspectives. *Cell Cycle* 8:391–393.
20. Klionsky DJ, Cuervo AM, Seglen PO (2007) Methods for monitoring autophagy from yeast to human. *Autophagy* 3:181–206.
21. Ahmed Z, Archer JR, Brown RA (1995) Cell proliferation within the growth plate of the tich mouse. *Bone* 16 (4, Suppl):305S–310S.
22. Walker JG, et al. (2006) Expression of Jak3, STAT1, STAT4, and STAT6 in inflammatory arthritis: Unique Jak3 and STAT4 expression in dendritic cells in seropositive rheumatoid arthritis. *Ann Rheum Dis* 65:149–156.
23. Hu X, Chen J, Wang L, Ivashkiv LB (2007) Crosstalk among Jak-STAT, Toll-like receptor, and ITAM-dependent pathways in macrophage activation. *J Leukoc Biol* 82:237–243.
24. Monari C, et al. (2009) A microbial polysaccharide reduces the severity of rheumatoid arthritis by influencing Th17 differentiation and proinflammatory cytokines production. *J Immunol* 183:191–200.
25. Richard M, Arfi A, Rhinn H, Gandolphe C, Scherman D (2008) Identification of new markers for neurodegeneration process in the mouse model of Sly disease as revealed by expression profiling of selected genes. *J Neurosci Res* 86:3285–3294.
26. Weaver AL (2004) Efficacy and safety of the anti-TNF biologic agents. *Mod Rheumatol* 14:101–112.
27. Strand V, Singh JA (2007) Improved health-related quality of life with effective disease-modifying antirheumatic drugs: Evidence from randomized controlled trials. *Am J Manag Care* 13 (Suppl 9):S237–S251.
28. Krzysiek R, et al. French Ankylosing Spondylitis Infliximab Network (2009) Circulating concentration of infliximab and response to treatment in ankylosing spondylitis: Results from a randomized control study. *Arthritis Rheum* 61:569–576.
29. Laharie D, et al. (2009) The tolerance and efficacy of a postponed retreatment with infliximab in Crohn's disease primary responders. *Aliment Pharmacol Ther* 29: 1240–1248.
30. Williams RO, Feldmann M, Maini RN (1992) Anti-tumor necrosis factor ameliorates joint disease in murine collagen-induced arthritis. *Proc Natl Acad Sci USA* 89: 9784–9788.
31. Boettger MK, et al. (2008) Antinociceptive effects of tumor necrosis factor alpha neutralization in a rat model of antigen-induced arthritis: Evidence of a neuronal target. *Arthritis Rheum* 58:2368–2378.
32. Nagasawa H, Kameda H, Sekiguchi N, Amano K, Takeuchi T (2009) Improvement of the HAQ score by infliximab treatment in patients with RA: Its association with disease activity and joint destruction. *Mod Rheumatol* 19:166–172.
33. van der Kooij SM, et al. (2009) Patient-reported outcomes in a randomized trial comparing four different treatment strategies in recent-onset rheumatoid arthritis. *Arthritis Rheum* 61:4–12.
34. Yavropoulou MP, Yovos JG (2008) Osteoclastogenesis—Current knowledge and future perspectives. *J Musculoskelet Neuronal Interact* 8:204–216.
35. Sands MS, Birkenmeier EH (1993) A single-base-pair deletion in the beta-glucuronidase gene accounts for the phenotype of murine mucopolysaccharidosis type VII. *Proc Natl Acad Sci USA* 90:6567–6571.
36. Poltorak A, et al. (2001) A point mutation in the IL-12R beta 2 gene underlies the IL-12 unresponsiveness of Lps-defective C57BL/10ScCr mice. *J Immunol* 167:2106–2111.
37. Poltorak A, et al. (1998) Defective LPS signaling in C3H/HeJ and C57BL/10ScCr mice: Mutations in Tlr4 gene. *Science* 282:2085–2088.
38. Yoshida M, Noguchi J, Ikadai H, Takahashi M, Nagase S (1993) Arylsulfatase B-deficient mucopolysaccharidosis in rats. *J Clin Invest* 91:1099–1104.
39. Kunieda T, et al. (1995) Mucopolysaccharidosis type VI in rats: Isolation of cDNAs encoding arylsulfatase B, chromosomal localization of the gene, and identification of the mutation. *Genomics* 29:582–587.
40. He X, Chen F, Gatt S, Schuchman EH (2001) An enzymatic assay for quantifying sphingomyelin in tissues and plasma from humans and mice with Niemann-Pick disease. *Anal Biochem* 293:204–211.
41. He X, Huang CL, Schuchman EH (2009) Quantitative analysis of sphingosine-1-phosphate by HPLC after napthalene-2,3-dicarboxaldehyde (NDA) derivatization. *J Chromatogr, B Anal Technol Biomed Life Sci* 877:983–990.